Plant Protection, 09 (04) 2025. 847-858 DOI:10.33804/pp.009.04.5898

Available Online at EScience Press
Plant Protection
ISSN: 2617-1287 (Online), 2617-1279 (Print)
http://esciencepress.net/journals/PP

Research Article

Green Synthesis of Zinc Oxide Nanoparticles Using *Zea mays* leaves: Characterization and Comparison of Antifungal Activity with Commercial and Bulk ZnO against *Aspergillus flavus*

Muna A. Alrawi, Halima Z. Hussein

Department of Plant Protection, College of Agriculture Engineering Science, University of Baghdad, Iraq.

ARTICLE INFO

Article history
Received: 18th August, 2025
Revised: 31st October, 2025
Accepted: 4th November, 2025

Keywords
Green nanotechnology
Zinc oxide nanoparticles
Zea mays leaf extract
Antifungal activity
Aspergillus flavus

ABSTRACT

Zinc oxide nanoparticles (ZnO NPs) have gained considerable attention due to their unique physicochemical properties and broad-spectrum antimicrobial activity, making them valuable in agricultural and biomedical applications. In this study, ZnO NPs were synthesized via a green synthesis approach using *Zea mays* (maize) leaf extract as both a reducing and stabilizing agent. The antifungal activity of the synthesized ZnO NPs was compared with that of commercial and conventionally produced ZnO samples against *Aspergillus flavus*. The synthesis process was monitored using ultraviolet-visible (UV-Vis) spectroscopy, which showed a distinct absorption peak at 308 nm, confirming the formation of ZnO nanoparticles. Fourier-transform infrared (FTIR) spectroscopy revealed characteristic Zn–O vibration peaks in the range of 430-450 cm^{-1}, indicating the crystallization of ZnO. X-ray diffraction (XRD) analysis exhibited sharp and well-defined peaks at specific 2θ angles, confirming the nanoscale hexagonal wurtzite crystal structure of ZnO. The average particle size, calculated using the Scherrer equation, was 177.46 nm for the green-synthesized ZnO NPs, smaller than that of commercial nano-ZnO (230.63 nm) and conventional bulk ZnO (253.66 nm), demonstrating the efficiency of the green synthesis method in reducing particle size. The antifungal bioassay against *A. flavus* revealed that the green-synthesized ZnO NPs exhibited the highest inhibitory effect, with 94.4% control, followed by commercial nano-ZnO (88.9%) and conventional ZnO (83.3%). These findings clearly indicate that green synthesis not only reduces particle size but also enhances antifungal efficacy. This environmentally friendly and efficient approach holds significant potential for the application of ZnO NPs in both agricultural and biomedical fields.

Corresponding Author: Muna A. Alrawi
Email: muna.abd2204p@coagri.uobaghdad.edu.iq

Introduction

The green synthesis of zinc oxide nanoparticles (ZnO NPs) involves a series of chemical reactions in which plant extracts act as both reducing and capping agents. ZnO NPs synthesized from *Zea mays* (maize) have been reported to exhibit superior efficiency, particle size control, and morphological characteristics compared to those derived from other botanicals such as *Eucalyptus*, *Aloe vera*, and *Juglans regia* (Mutukwa et al., 2022; Ali et al., 2023; Adeningrum et al., 2025).

The leaves of *Zea mays* are rich in phytochemicals such as phenolics, flavonoids, terpenoids, and proteins, which

donate electrons to zinc precursors and stabilize the nascent nuclei, thereby facilitating nanoparticle formation and colloidal stability. Both aqueous and ethanolic maize leaf extracts have been shown to promote the nucleation and growth of ZnO NPs (Iravani, 2011; Ali et al., 2023; Naseer et al., 2023; Al-Darwesh et al., 2024).

Phenolic compounds serve as the primary reducing agents in the synthesis process by donating electrons to zinc ions, facilitating their reduction (Awasthi et al., 2023; Naseer et al., 2023). Flavonoids also contribute by forming complexes with metal ions, stabilizing the nanoparticles, and preventing aggregation (Hamed et al., 2023; Ali and Baghdadi, 2024). Terpenoids, particularly those containing hydroxyl groups, participate in both reduction and stabilization of zinc ions (Awasthi et al., 2023; Al-Darwesh et al., 2024). Proteins and amino acids act as capping agents, binding to the nanoparticle surface and stabilizing them in the colloidal solution (Hajinasiri et al., 2016; Ali et al., 2023; Hamed et al., 2023; Javad et al., 2024).

The phytochemicals present in the extract react with zinc ions (Zn^{2+}) from zinc salt precursors, such as zinc nitrate hexahydrate, resulting in the reduction of Zn^{2+} to metallic zinc nanoparticles (Zn^0). This reduction is facilitated by hydroxyl (-OH) and carbonyl (C=O) functional groups within the plant extract. The reduced zinc atoms subsequently nucleate and grow into nanoparticles (Ali and Baghdadi, 2024; Villagrán et al., 2024). Under ambient conditions, the metallic zinc nanoparticles may oxidize to form ZnO NPs, which are more stable and possess enhanced functional properties for diverse applications (Rani and Shanker 2021; Ahmed et al., 2024).

Several factors influence the biosynthesis of ZnO NPs from *Z. mays* leaves. The pH of the reaction medium significantly affects nanoparticle formation, while higher temperatures accelerate the reaction rate. The concentration of plant extract and reaction duration determine particle size and dispersion. Prolonged reaction times can lead to larger particles due to Ostwald ripening (Raghupathi et al., 2011; Bala et al., 2015; Kumar et al., 2025).

Characterization of ZnO NPs synthesized from maize leaves involves various analytical techniques to determine their structural, morphological, and optical properties. UV-Visible spectrophotometry is used to confirm nanoparticle formation by detecting the surface plasmon resonance (SPR) peak in the UV-VIS region. X-ray diffraction (XRD) analysis reveals the crystalline nature of the nanoparticles, typically confirming the hexagonal wurtzite structure of ZnO. Fourier-transform infrared (FTIR) spectroscopy identifies functional groups (e.g., hydroxyl and carbonyl) associated with biomolecules responsible for nanoparticle stabilization (Hoseinpour et al., 2017; Zelekew et al., 2021; Karam and Abdulrahman, 2022).

The synthesis process using *Z. mays* leaves is simple, cost-effective, and does not require complex equipment or high-energy inputs, making it suitable for both research and industrial applications (Ali et al., 2023; Hamed et al., 2023). The use of plant extracts eliminates the need for toxic chemicals and excessive energy consumption, making this approach environmentally sustainable (Elshafie et al., 2023; Janani et al., 2024).

ZnO NPs have broad agricultural applications. They can act as nanofertilizers to enhance crop growth and yield and as protective agents against plant pathogens and pests (Tamim et al., 2023; Parmar, 2024; Arain et al., 2025).

The antifungal mechanism of ZnO NPs primarily involves the generation of reactive oxygen species (ROS), including hydrogen peroxide (H_2O_2), hydroxyl radicals (•OH), and superoxide anions (O_2^-). These ROS induce oxidative stress in fungal cells, leading to cell wall damage, membrane disruption, and DNA degradation, thereby impairing cellular homeostasis and promoting cell death (Savi et al., 2013; Gacem et al., 2021; Ikhechi et al., 2021; Dhiman et al., 2022). ZnO NPs also interact with fungal membranes, increasing permeability and causing leakage of intracellular contents such as ions, proteins, and metabolites. Furthermore, they interfere with the synthesis of chitin and other structural components, disrupting the integrity of the cell wall (Li et al., 2017; Benková et al., 2024).

ZnO NPs can further alter ion homeostasis within fungal cells by affecting the transport of essential ions (Zn^{2+}, K^+, and Ca^{2+}) and inhibiting key enzymatic activities involved in cell wall synthesis and energy metabolism, thereby impairing fungal growth and survival (Patiño-Portela et al., 2021; Subba et al., 2024).

ZnO NPs have demonstrated strong antifungal activity against *Aspergillus flavus*, a major aflatoxin-producing pathogen. Several studies have confirmed their efficacy, either alone or in combination with other materials, in suppressing fungal growth and aflatoxin production (Hernández-Meléndez et al., 2018; Fathima et al., 2020; Dutta et al., 2021; Achilonu et al., 2024). ZnO NPs synthesized using *Chlorella vulgaris* exhibited significant

inhibition zones (50 mm and 14 mm) against azole-resistant *A. flavus* isolates from white and yellow maize, respectively (Alhazmi and Sharaf, 2023). Similarly, ZnO NPs biosynthesized from lemongrass leaf extract inhibited 92.25% of *A. flavus* growth and completely suppressed aflatoxin production at specific concentrations, demonstrating their potential as eco-friendly antifungal agents (Kumari et al., 2019; Janani et al., 2024).

The antifungal efficacy of ZnO NPs has also been linked to the downregulation of key genes involved in aflatoxin biosynthesis, as reported in studies employing quantum dot ZnO (Bastami et al., 2024). However, limited studies have explored the use of *Z. mays* leaf extract for the biosynthesis of ZnO NPs and their antifungal potential against *A. flavus*. Therefore, the present study aims to synthesize and characterize ZnO NPs using *Z. mays* leaf extract and evaluate their antifungal efficacy in comparison with commercial and bulk ZnO.

Materials and Methods

Collection and preparation of plant extract

Fresh and healthy leaves of *Z. mays* were collected from a pesticide-free field and thoroughly washed under running tap water to remove dust and surface contaminants. Subsequently, the leaves were rinsed three times with distilled water to ensure complete removal of impurities. After washing, 100 g of fresh leaves were weighed using an analytical balance, chopped into small pieces, and placed in an electric blender containing 100 ml of distilled water. The mixture was blended for 2-3 min until a uniform, homogeneous slurry was obtained.

The homogenized mixture was then transferred to a 500 ml beaker and subjected to heating at 60-70°C for 30 min using a magnetic stirrer with continuous stirring to facilitate the extraction of bioactive phytochemicals. After heating, the mixture was allowed to cool at room temperature and then filtered through sterile muslin cloth to remove large debris and fibrous material. The filtrate, representing the crude aqueous leaf extract, was collected for nanoparticle synthesis. The remaining residue was centrifuged at 10,000 rpm for 15 min to recover any suspended particles, and the supernatant was combined with the filtrate to obtain a clear extract.

Preparation of zinc nitrate solution

To prepare the precursor solution, 5.95 g of zinc nitrate hexahydrate ($Zn(NO_3)_2 \cdot 6H_2O$) were accurately weighed and dissolved in 100 ml of distilled water in a clean beaker. The solution was then transferred to a 200 ml volumetric flask and diluted to the mark with distilled water to achieve a final concentration of 0.1 M $Zn(NO_3)_2$ solution. The prepared solution was stored in an amber bottle to prevent light-induced degradation prior to use.

Green synthesis of zinc oxide nanoparticles (ZnO NPs)

For the green synthesis of ZnO nanoparticles, 100 ml of the freshly prepared *Z. mays* leaf extract was slowly added to 100 ml of the 0.1 M $Zn(NO_3)_2$ solution under continuous stirring on a magnetic hot plate. The reaction mixture was maintained at 60-70°C with constant stirring for 2 h to ensure uniform mixing and complete reduction of zinc ions. A gradual change in color of the solution, from pale green to light yellow and finally to milky white, was observed, indicating the formation of ZnO NPs (Mohammadi et al., 2018; Cervantes-Gaxiola et al., 2024; Vignesh, 2025).

After completion of the reaction, the mixture was cooled to room temperature and centrifuged at 10,000 rpm for 15 min to collect the ZnO NP precipitate. The obtained pellet was washed three times with distilled water and ethanol to remove any unreacted biological residues. The final product was dried in a hot air oven at 60°C overnight, ground into fine powder using a mortar and pestle, and stored in airtight containers for further characterization and bioassay.

Characterization of synthesized ZnO NPs

The optical properties of the synthesized ZnO NPs were evaluated using a UV-Visible spectrophotometer within the wavelength range of 200-600 nm to confirm nanoparticle formation. Fourier Transform Infrared (FTIR) spectroscopy was employed to identify the functional groups in the *Z. mays* leaf extract responsible for the reduction and stabilization of ZnO NPs by detecting specific molecular vibrations.

To determine the crystalline structure and phase purity of the nanoparticles, X-ray diffraction (XRD) analysis was performed. The XRD pattern provided distinct diffraction peaks, which were compared with standard ZnO reference data to confirm the crystalline nature and absence of impurities. The average crystallite size (D) of the ZnO NPs was calculated using the Scherrer equation:

$$D = \frac{K\lambda}{\beta \cos\theta}$$

Where K is the shape factor (0.9), λ is the X-ray wavelength, β is the full width at half maximum (FWHM) of the diffraction peak, and θ is the Bragg's diffraction angle (Baskar et al., 2013; Shinde, 2015).

Preparation of potato dextrose agar (PDA) medium and antifungal bioassay

For the antifungal assay, 39 g of PDA powder were dissolved in one liter of distilled water. The medium was sterilized in an autoclave at 121°C and 15 psi pressure for 15 minutes. After sterilization, the molten PDA was allowed to cool to 45-50°C, an optimal temperature for incorporating treatments without affecting the consistency of the agar or the bioactivity of the compounds.

The ZnO NPs were suspended in sterile distilled water using an ultrasonic bath to achieve uniform dispersion and minimize nanoparticle agglomeration. This step ensured even distribution of nanoparticles within the agar medium. The desired concentrations of ZnO NPs were then incorporated into the PDA medium according to the experimental design.

Table 1 summarizes the various treatments and preparation methods applied for the antifungal evaluation of ZnO NPs synthesized from *Z. mays* leaf extract.

Table 1. Types of treatments used and their preparation methods for evaluating the antifungal efficacy of different forms of zinc oxide.

Treatment No.	Treatment type	Medium
1	Green synthesis ZnO NPs	Prepared form zea mays leaves 0.1 M
2	ZnO NPs 50 nm	Wight 100 mg suspend in 10 ml distilled water and use Ultrasonic for 15 min to ensure dispersion.
3	ZnO)bulk)	Wight 100 mg suspend in 10 ml distilled water mix and use Ultrasonic for 15 min to ensure dispersion
4	control	No added

Evaluation of the antifungal efficacy of different forms of zinc oxide

Preparation of treatment media

To assess the antifungal efficacy of different forms of zinc oxide (ZnO), three types of ZnO preparations were evaluated: (i) green-synthesized ZnO-NPs, (ii) chemically synthesized ZnO nanoparticles, and (iii) bulk ZnO powder. For each treatment, appropriate suspensions were prepared in sterile distilled water.

For the preparation of the treatment media, 1 ml of each respective ZnO suspension was added to 100 ml of sterilized, molten PDA medium maintained at approximately 45-50°C. The medium was stirred thoroughly to ensure a uniform distribution of the ZnO materials throughout the agar. Approximately 20 ml of the treated medium was then poured into each sterile Petri dish under aseptic conditions. Control plates were prepared in the same manner but without the addition of any ZnO formulation.

Inoculation and incubation

After solidification of the medium, a 5-mm-diameter mycelial disc from the actively growing margin of a *A. flavus* culture (7-day-old colony) was aseptically placed at the center of each Petri plate. For each treatment, three replicates were prepared to allow statistical comparison among treatments. The inoculated plates were incubated at 28 ± 2°C for seven days under dark conditions.

Measurement of fungal growth

The radial growth of *A. flavus* colonies was recorded daily by measuring the colony diameter along two perpendicular axes, and the mean value was calculated. The percentage inhibition of mycelial growth in each treatment was determined relative to the control using the following formula:

$$\text{Inhibition (\%)} = \frac{C - T}{C} \times 100$$

Where C represents the average colony diameter in the control and T represents the average colony diameter in the treatment.

Statistical analysis

Data were subjected to analysis of variance (ANOVA) using a completely randomized design (CRD). Means were compared using the Least Significant Difference (LSD) test at a 5% probability level ($p \leq 0.05$) to determine significant differences among treatments in antifungal activity.

Results and Discussion

The UV-Vis absorption spectrum of the synthesized nanoparticles exhibited a sharp absorption peak at 308 nm, confirming the successful formation of ZnONPs. This observation is consistent with previous reports that documented a similar absorption peak in the same range (Naiel et al., 2022), as shown in Figure 1. The absorption peak in the ultraviolet (UV) region

corresponds to electronic transitions from the valence band to the conduction band in ZnO. The presence of this peak is attributed to the characteristic band gap of ZnO and serves as a reliable indicator of the purity and quality of the synthesized nanoparticles, as presented in Table 2.

The results obtained from the X-ray diffraction analysis of the three samples, green-synthesized ZnO NPs, ZnO NPs (50 nm), and commercial ZnO, provided understandings about the crystal and nanostructural properties of the materials. The XRD pattern (Figure 2) showed the diffraction intensity (vertical axis) as a function of the diffraction angle (2θ, horizontal axis). The peaks in the diffraction pattern represented specific planes within the crystalline structure where constructive interference of X-rays occurred.

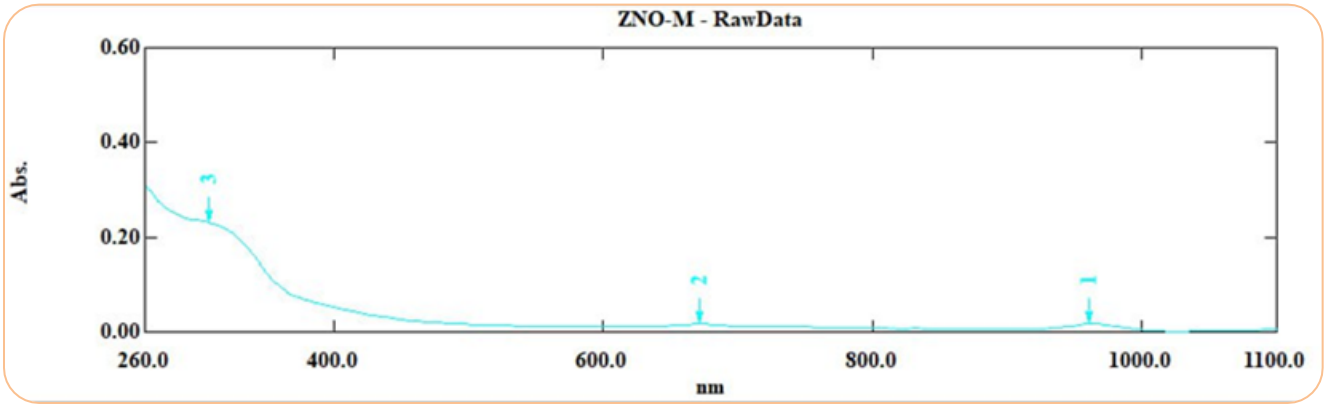

Figure 1. UV-Vis spectrum of the green-synthesized ZnO nanoparticles.

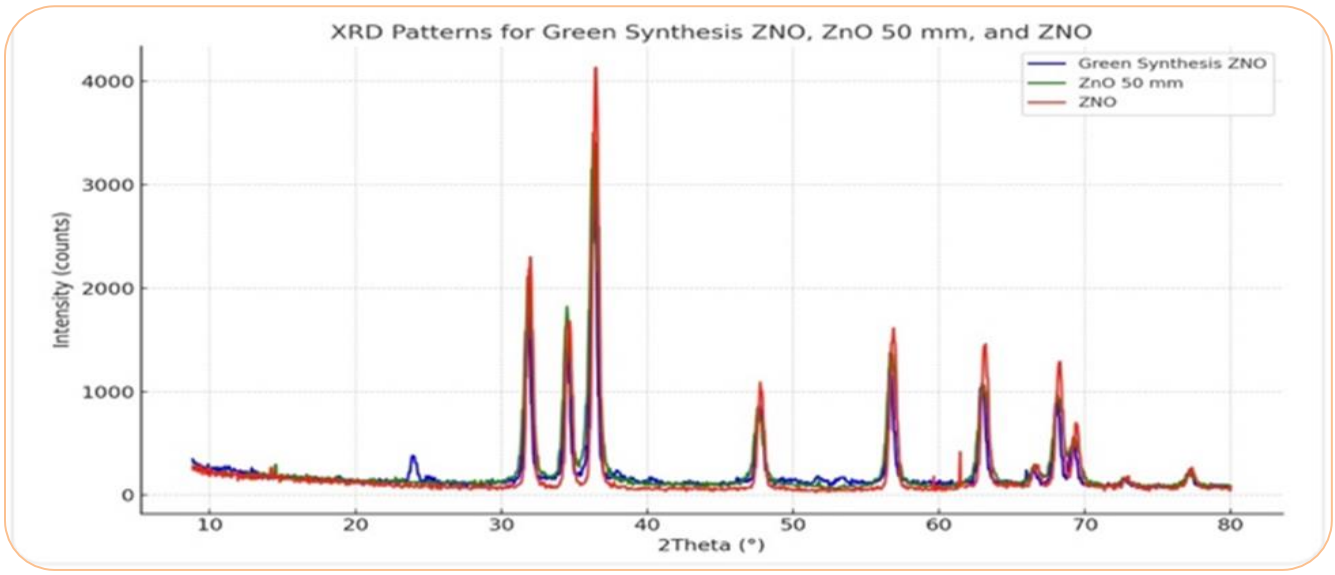

Figure 2. XRD patterns of ZnO samples synthesized by different methods: green synthesis, 50 nm ZnO, and bulk ZnO.

Table 2. Absorbance peaks of ZnO nanoparticles and their interpretation based on UV, visible, and NIR bands.

Peak No.	Wavelength (nm)	Absorption	Details
1	961.0	0.018	Absorption in the near-infrared (NIR) region, which may be related to impurities or defects in the crystal structure.
2	672.0	0.017	Absorption in the visible region, which may be related to electron transitions resulting from defect centers or oxygen centers.
3	308.0	0.231	Absorption in the UV region, this peak is very important because it indicates the band gap in ZnO.

In the green-synthesized ZnO NPs, several distinct peaks were observed at 2θ values ranging from 20° to 80°, with the most intense peak appearing at 36.27° 2θ. This indicated the presence of crystalline material at that position. The overall intensity varied between low and high values, suggesting variations in crystal density within the sample.

For the ZnO NPs (50 nm) sample, a prominent diffraction peak was detected at 36.41° 2θ with an intensity of 3291.92, indicating a more pronounced crystalline structure compared to the green-synthesized ZnO NPs. In the commercial ZnO sample, the main diffraction peak appeared at 36.47° 2θ with an even higher intensity of 4108.62, suggesting a higher degree of crystal organization. The crystallite size of each sample was subsequently calculated using the Scherrer equation based on the obtained XRD data, and calculated values are presented in table in (Table 3).

The FTIR spectra of the three samples (green-synthesized ZnO, ZnO 50 nm, and ZnO bulk) (Table 4) showed characteristic peaks in the 400-600 cm^{-1} range, confirming the presence of Zn-O bonds typical of the ZnO crystalline structure. However, peaks observed in the 1000-1500 cm^{-1} range indicated the presence of C–H bonds, which might have resulted from organic residues remaining from the green synthesis process or from organic impurities. Water or moisture absorption peaks appeared in the 1600-1700 cm^{-1} and 3000-3500 cm^{-1} ranges, suggesting the possible absorption of moisture from the environment or the presence of water molecules bound to the nanostructured surface. These bands are presented in (Figure 3).

Table 3: Estimation of average nanoscale size of ZnO particles using the Scherrer equation based on XRD data.

Sample	Average nanoscale size
Green synthesis ZnO NPs	177.46
ZnO NPs 50 nm	230.63
ZnO)bulk)	253.66

Surface morphology of ZnO NPs

The surface morphology and particle size of ZnO NPs synthesized by different methods were examined using Field Emission Scanning Electron Microscopy (FE-SEM) (Figure 4). The micrographs revealed distinct morphological variations among the samples. Green-synthesized ZnO NPs using *Z. mays* leaf extract exhibited a uniform, quasi-spherical morphology with particle sizes ranging from approximately 30-90 nm. The nanoparticles appeared well-dispersed with minimal agglomeration, confirming the stabilizing role of phytochemicals such as phenolics and flavonoids in controlling nucleation and growth during synthesis.

Table 4. FTIR analysis of ZnO samples prepared by different methods showing the distribution of functional absorption bands.

Sample	Range (cm^{-1})	Peaks (cm^{-1})	Functional group or association	Notes
Green synthesis ZnO NPs	400-600	430-450	Zn-O	Vibration of Zn-O bonds in the crystal lattice
Green synthesis ZnO NPs	1000-1500	1300-1500	C-H	Presence of organic compounds from the synthesis process
Green synthesis ZnO NPs	1600-1700	1620	O-H	water or moisture absorption
Green synthesis ZnO NPs	3000-3500	3400-3500	O-H	Water adsorbed on the surface of the particles
ZnO NPs 50 nm	400-600	430-450	Zn-O	Zn-O lattice vibration
ZnO NPs 50 nm	1000-1500	1400-1500	C-H	organic matter residues
ZnO NPs 50 nm	1600-1700	1640	O-H	bound water
ZnO NPs 50 nm	3000-3500	3450	O-H	Water adsorbed on the surface of the particles
ZnO)bulk)	400-600	430-450	Zn-O	Zn-O vibrations
ZnO)bulk)	1000-1500	1320-1450	C-H	organic matter residues
ZnO)bulk)	1600-1700	1650	O-H	bound water
ZnO)bulk)	3000-3500	3410-3480	O-H	absorbed water

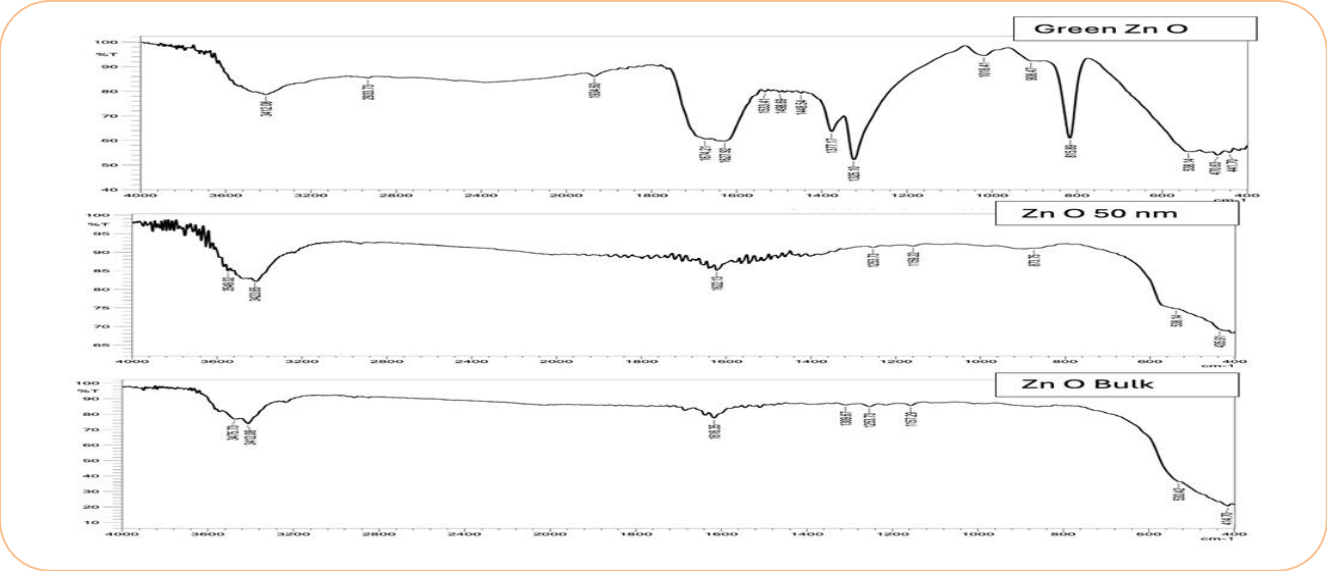

Figure 3. FTIR analysis of ZnO samples synthesized by different methods showing characteristic functional bonds and chemical structures.

In contrast, the commercially available ZnO NPs displayed a more heterogeneous size distribution, with noticeable particle clustering and irregular boundaries, indicating aggregation during processing. The bulk ZnO sample showed large, rod-like and irregular particles exceeding 100 nm, confirming the absence of nanoscale features. These morphological observations demonstrate that the green synthesis approach effectively reduces particle size and enhances surface uniformity compared with conventional methods. The nanoscale dimensions and homogeneous distribution of green-synthesized ZnO NPs are expected to improve their antifungal efficiency by increasing the surface area, active reactive sites, and contact interaction with fungal hyphae, as supported by previous studies (Raghupathi et al., 2011; Bala et al., 2015; Al-Darwesh et al., 2024).

Antifungal activity of ZnO NPs

When comparing the antifungal efficacy of biosynthesized, commercial, and bulk ZnO, as presented in Table 5, the green-synthesized ZnO NPs showed the highest inhibition of *A. flavus* (94.4 ± 1.1%) with a mean colony diameter of 5.0 ± 0.3 mm, followed by commercial ZnO NPs (88.9 ± 0.8%) and bulk ZnO (83.3 ± 1.3%). The differences among treatments were statistically significant ($LSD_{0.05}$ = 0.672). Visual confirmation of fungal growth suppression is shown in Figure 5.

One-way ANOVA performed on fungal growth diameter indicated significant differences among treatments, confirming that all three (bulk ZnO, commercial ZnO NPs, and green-synthesized ZnO NPs) caused significant inhibition compared with the control. Moreover, the green-synthesized ZnO NPs exhibited superior antifungal activity over the other two treatments ($p < 0.001$). This enhanced efficacy may be attributed to the smaller particle size resulting from green synthesis and the presence of residual phenolic or flavonoid compounds on the nanoparticle surface, which may confer additional antifungal properties (Kumari et al., 2019).

Previous studies have demonstrated that ZnO NPs exert antifungal activity primarily through the generation of ROS, which damage cell membranes and intracellular components (Alhazmi et al., 2023). Furthermore, smaller nanoparticles have a greater capacity to penetrate fungal cell walls, thereby enhancing their inhibitory potential (Wu et al., 2025).

Comparable findings were reported by Alhazmi and Sharaf (2023), who observed inhibition zones of up to 50 mm using plant-mediated ZnO NPs against resistant isolates of *A. flavus*. Other studies have indicated that nanoparticles can also reduce aflatoxin production by modulating the gene expression of enzymes involved in toxin biosynthesis (Rodrigues et al., 2021; Gobikanila and Jeyaramraja, 2024). These results are consistent with previous and recent reports showing that ZnO NPs, irrespective of the synthesis method, exhibit potent antifungal activity against various fungal species, with green-synthesized ZnO NPs displaying superior efficacy (Djearamane et al., 2022; Raza et al., 2024; Truong and Le, 2024).

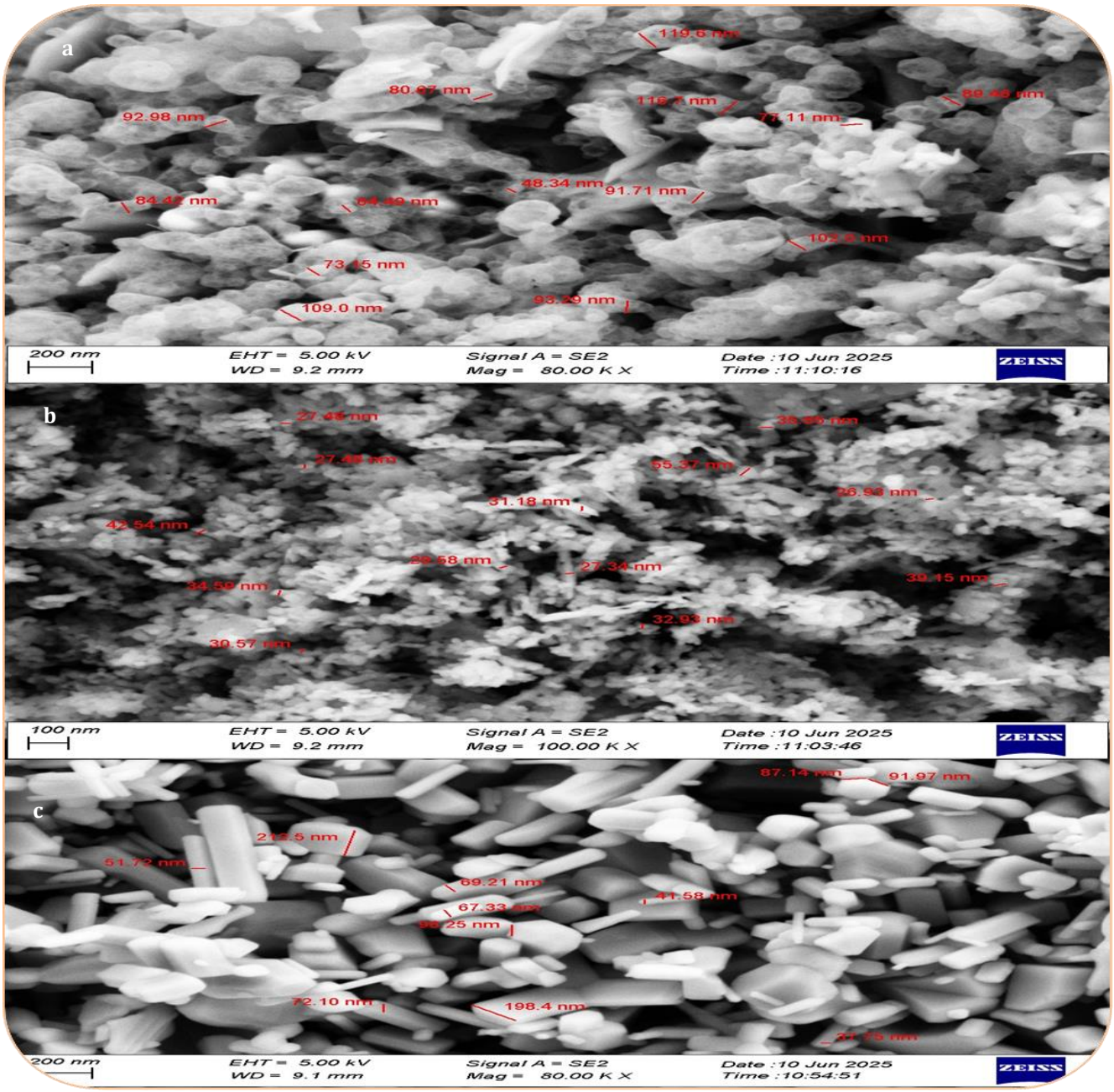

Figure 4. FE-SEM micrographs showing the surface morphology and particle size distribution of ZnO nanoparticles synthesized by different methods: (a) green-synthesized ZnO NPs, (b) commercial ZnO NPs, and (c) bulk ZnO NPs.

Table 5. Comparison of the effects of ZnO prepared by different methods on the growth inhibition of *A. flavus* (mean ± SD, n = 3).

Treatment	Fungal growth diameter mm	Inhibition rate	± SD
control	90 mm	0 %	± 0.0
Green synthesis ZnO NPs	5 mm	94.4 %	± 1.1
ZnO NPs 50 nm	10 mm	88.9 %	± 0.8
ZnO)bulk)	15 mm	83.3 %	± 1.3
LSD (0.05)	0.672		-

Note: Tested concentration = 100 µg/ml. Data were analyzed by one-way ANOVA followed by LSD test ($p \leq 0.05$).

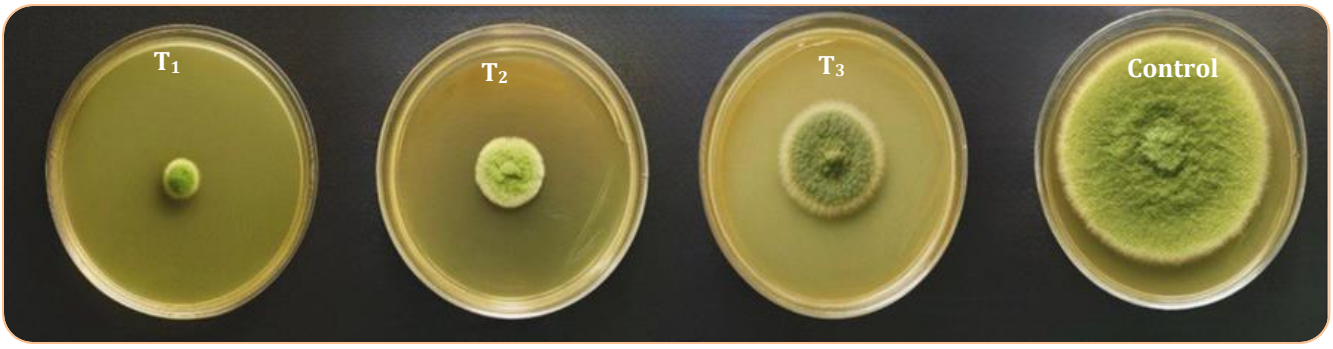

Figure 5. Comparison of the effects of green-synthesized ZnO, ZnO (50 nm), and bulk ZnO on fungal growth.

Conclusion

The study confirmed that ZnO NPs synthesized using *Z. mays* leaf extract exhibited a smaller average particle size (177.46 nm) compared to conventionally and commercially prepared ZnO samples. The reduced size increased the effective surface area, thereby enhancing their antifungal performance. The results demonstrated that the green synthesis approach not only reduced particle size but also improved the uniformity and crystallinity of the nanoparticles, resulting in greater antifungal efficacy against *A. flavus*.

Characterization analyses (XRD and FTIR) verified the hexagonal wurtzite structure and the presence of regular Zn–O bonds, indicating their nanoscale nature and structural stability. Overall, these findings demonstrate that *Z. mays* is an effective and sustainable bioresource for producing antifungal ZnO NPs.

Future work should focus on evaluating the long-term stability of these nanoparticles under variable environmental conditions (e.g., humidity and temperature) and assessing their antimicrobial potential against a broader spectrum of pathogenic fungi and bacteria. Moreover, detailed investigations are recommended to elucidate the relationship between particle size and biological activity to optimize their applications in agricultural and biomedical fields.

Authors' Contributions

MAA conceptualized and designed the study, carried out the experimental work including the green synthesis of nanoparticles and antifungal bioassays, collected and statistically analyzed the data, and prepared the initial draft of the manuscript; HZH provided overall supervision, guidance, and essential laboratory resources, critically evaluated the scientific content, and contributed substantially to the writing, review, and refinement of the manuscript; Both authors engaged in constructive discussions throughout the research process, ensured the accuracy and integrity of the data, and approved the final version of the manuscript for publication.

Research Funding

This research did not receive any grant from funding agencies.

Conflict of Interest

The authors declare no conflict of interest.

Sustainable Development Goals Targeted

SDG 3: Good Health and Well-being
SDG 12: Responsible Consumption and Production
SDG 15: Life on Land

Reference

Achilonu, C.C., Kumar, P., Swart, H.C., Roos, W.D., Marais, G.J., 2024. Zinc oxide: Gold nanoparticles (ZnO: Au NPs) exhibited antifungal efficacy against *Aspergillus niger* and *Aspergillus candidus*. BioNanoScience, 14, 799-813.

Adeningrum, D., Rosa, A., Wahyusi, K., Yogaswara, R., 2025. Biosintesis nanopartikel ZnO menggunakan ekstrak daun tanaman jagung (*Zea mays* L.). Jurnal Fisika Unand 14(2), 160-166.

Ahmed, I., Mir, F.A., Bhat, M., Aasif, M., Yatoo, G.N., Banday, J., 2024. Characterization and antimicrobial properties of zinc oxide nanoflakes prepared via green chemistry method using corn silk extract of *Zea mays*. ChemistrySelect 9(13), e202305130.

Al-darwesh, M.Y., Ibrahim, S.S., Mohammed, M.A., 2024. A Review on plant extract mediated green synthesis of zinc oxide nanoparticles and their

biomedical applications. Results in Chemistry 7, 101368.

Alhazmi, N.M., Sharaf, E.M., 2023. Fungicidal activity of zinc oxide nanoparticles against azole-resistant *Aspergillus flavus* isolated from yellow and white maize. Molecules, 28, 711.

Ali, M.B., Elmnasri, K., Haq, S., Shujaat, S., Hfaiedh, M., Abdallah, F.B., Hedfi, A., Mahmoudi, E., Hamouda, B., Attia, M.B., 2023. *Zea mays*-mediated fabrication and characterization of zinc oxide nanoparticles with enhanced antibacterial and antioxidant properties. Digest Journal of Nanomaterials and Biostructures 18(4), 1577-1585.

Arain, J.A., Solangi, A.R., Depar, N., 2025. Evaluating yield and quality of wheat grains under single and integrated use of chemical and nano zinc fertilizers. Pakistan Journal of Botany, 57, 5.

Awasthi, G., Maheshwari, T., Sharma, R., Kumawat, T.K., Singh, G., Lodha, P., 2023. Actions and reactions of plant-derived zinc oxide nanoparticles. Materials Today: Proceedings, 95, 77-87.

Bala, N., Saha, S., Chakraborty, M., Maiti, M., Das, S., Basu, R., Nandy, P., 2015. Green synthesis of zinc oxide nanoparticles using *Hibiscus subdariffa* leaf extract: Effect of temperature on synthesis, antibacterial activity and antidiabetic activity. RSC Advances 5, 4993-5003.

Baskar, G., Chandhuru, J., Fahad, K.S., Praveen, A.S., 2013. Mycological synthesis, characterization and antifungal activity of zinc oxide nanoparticles. Asian Journal of Pharmacy and Technology 3, 142-146.

Bastami, N., Nikaein, D., Malakootikhah, J., Akbarein, H., Sharifzadeh, A., Haddadi, S., Khosravi, A.R., 2025. Effects of quantum dot zinc oxide, nano zinc oxide and zinc oxide on gene expression and aflatoxin production by *Aspergillus flavus* ATCC50041. Journal of Poultry Sciences and Avian Diseases 3, 1-12.

Benkova, D., Dishliyska, V., Staleva, J., Kostadinova, A., Staneva, G., Fawzy El-Sayed, K.M., Elshoky, H.A., Krumova, E., 2024. CS and ZnO nanoparticles as fungicides against potato fungal pathogens *Alternaria solani* and *Fusarium solani*: Mechanism underlining their antifungal activity. Comptes Rendus de l'Académie Bulgare des Sciences 77, 7.

Cervantes-Gaxiola, M.E., Vázquez-González, F.A., Rios-Iribe, E.Y., Méndez-Herrera, P.F., Leyva, C., 2024. Effect of pH on the green synthesis of ZnO nanoparticles using *Sorghum bicolor* seed extract and their application in photocatalytic dye degradation. Materials Letters 372, 136982.

Dhiman, S.C., Varma, A., Prasad, R., Goel, A., 2022. Mechanistic insight of the antifungal potential of green synthesized zinc oxide nanoparticles against *Alternaria brassicae*. Journal of Nanomaterials 2022, 1-13.

Djearamane, S., Xiu, L., Wong, L., Rajamani, R., Bharathi, D., Kayarohanam, S., De Cruz, A., Tey, L., Janakiraman, A., Aminuzzaman, M., Selvaraj, S., 2022. Antifungal properties of zinc oxide nanoparticles on *Candida albicans*. Coatings 12(12), 1864.

Dutta, P., Das, G., Boruah, S., Kumari, A., Mahanta, M., Yasin, A., Deb, L., 2021. Nanoparticles as nano-priming agents for antifungal and antibacterial activity against plant pathogens. Biological Forum International Journal 13, 476-482.

Elshafie, H.S., Osman, A., El-Saber, M.M., Camele, I., Abbas, E., 2023. Antifungal activity of green and chemically synthesized ZnO nanoparticles against *Alternaria citri*, the causal agent of citrus black rot. The Plant Pathology Journal 39, 265-274.

Fathima, A.F., Mani, R.J., Sakthipandi, K., Manimala, K., Hossain, A., 2020. Enhanced antifungal activity of pure and iron-doped ZnO nanoparticles prepared in the absence of reducing agents. Journal of Inorganic and Organometallic Polymers and Materials 30, 2397-2405.

Gacem, M.A., Terzi, V., Ould-El-Hadj-Khelil, A., 2021. Zinc Nanostructures: Detection and Elimination of Toxigenic Fungi and Mycotoxins. Elsevier, 403-430.

Gobikanila, K., Jeyaramraja, P., 2024. The use of silver nanoparticles against aflatoxin contamination in crops - mechanism, challenges and future scope. World Mycotoxin Journal 17(3-4), 161-176.

Ali, B.H., Baghdadi, M., 2024. A review of plant-derived metallic nanoparticles synthesized by biosynthesis: synthesis, characterization, and applications. Green and Sustainable Approaches Using Wastes for the Production of Multifunctional Nanomaterials, 251-272.

Hajinasiri, R., Norozi, B., Ebrahimzadeh, H., 2016. Biosynthesis of ZnO nanoparticles using corn silk of *Zea mays* L. extract. Chemistry Letters 45, 1238-1240.

Hamed, R., Obeid, R.Z., Abu-Huwaij, R., 2023. Plant-mediated green synthesis of zinc oxide

nanoparticles: an insight into biomedical applications. Nanotechnology Reviews 12.

Hernández-Meléndez, D., Salas-Téllez, E., Zavala-Franco, A., Tellez, G., Méndez-Albores, A., Vázquez-Durán, A., 2018. Inhibitory effect of flower-shaped zinc oxide nanostructures on the growth and aflatoxin production of a highly toxigenic strain of *Aspergillus flavus*. Materials 11, 1265.

Hoseinpour, V., Souri, M., Ghaemi, N., Shakeri, A., 2017. Optimization of green synthesis of ZnO nanoparticles by *Dittrichia graveolens* (L.) aqueous extract. Health Biotechnology and Biopharma 1(2), 39-49.

Ilkhechi, N., Mozammel, M., Khosroushahi, A.Y., 2021. Antifungal effects of ZnO-TiO_2/Au nanostructures on *Aspergillus flavus*. Journal of the Australian Ceramic Society 57, 793-802.

Iravani, S., 2011. Green synthesis of metal nanoparticles using plants. Green Chemistry 13, 2638-2650.

Janani, M., Viswanathan, D., Pandiaraj, S., Govindasamy, R., Gomathi, T., Vijayakumar, S., 2024. Review on phyto-extract methodologies for procuring ZnO NPs and their pharmacological functionalities. Process Biochemistry 147, 186-212.

Javad, S., Singh, A., Kousar, N., Arifeen, F., Nawaz, K., Azhar, L., 2024. Zinc-based nanofertilizers: synthesis and toxicity assessments. Elsevier, 213-232.

Karam, S.T., Abdulrahman, A.F., 2022. Green synthesis and characterization of ZnO nanoparticles by using thyme plant leaf extract. Photonics 9, 594.

Kumar, N., Singh, A., Devra, V., 2025. Experimental investigation on plant extract-induced biosynthesis of nickel nanoparticles. Next Nanotechnology 7, 100104.

Kumari, P., Kumar, H., Kumar, J., Sohail, M., Singh, K., Prasad, K., 2019. Biosynthesized zinc oxide nanoparticles control the growth of *Aspergillus flavus* and its aflatoxin production. International Journal of Nano Dimension 10, 320-329.

Li, J., Sang, H., Guo, H., Popko, J.T., He, L., White, J.C., Dhankher, O.P., Jung, G., Xing, B., 2017. Antifungal mechanisms of ZnO and Ag nanoparticles to *Sclerotinia homoeocarpa*. Nanotechnology 28, 155101.

Mohammadi, F.M., Ghasemi, N., 2018. Influence of temperature and concentration on biosynthesis and characterization of zinc oxide nanoparticles using cherry extract. Journal of Nanostructure in Chemistry, 8, 93-102.

Mutukwa, D., Taziwa, R., Khotseng, L., 2022. A review of the green synthesis of ZnO nanoparticles utilising southern african indigenous medicinal plants. Nanomaterials 12.

Naiel, B., Fawzy, M., Halmy, M.W.A., Mahmoud, A.E.D., 2022. Green synthesis of zinc oxide nanoparticles using sea lavender (*Limonium pruinosum* L. Chaz.) extract: characterization, evaluation of anti-skin cancer, antimicrobial and antioxidant potentials. Scientific Reports 12(1), 20370.

Naseer, I., Javed, S., Shah, A.A., Tariq, A., Ahmad, A., 2023. Influence of phyto-mediated zinc oxide nanoparticles on growth of *Zea mays* L. Pakistan Journal of Botany 56(3), 911-923.

Parmar, K.M., 2024. Green synthesis of zinc oxide nanoparticles and its application as a green fertilizer in agriculture. The Holistic Approach to Environment 14, 109-113.

Patino-Portela, M.C., Arciniegas-Grijalba, P.A., Mosquera-Sanchez, L.P., Sierra, B.E.G., Munoz-Florez, J.E., Erazo-Castillo, L.A., Rodriguez-Paez, J.E., 2021. Effect of method of synthesis on antifungal ability of ZnO nanoparticles: chemical route vs green route. Advances in Nano research 10(2), 191-210.

Raghupathi, K.R., Koodali, R.T., Manna, A.C., 2011. Size-dependent bacterial growth inhibition and mechanism of antibacterial activity of zinc oxide nanoparticles. Langmuir 27, 4020-4028.

Rani, M., Shanker, U., 2021. Biogenic synthesis of zinc nanostructures: Characterization and mechanisms. In: Zinc-Based Nanostructures for Environmental and Agricultural Applications. Elsevier, pp. 65-91.

Raza, A., Malan, P., Ahmad, I., Khan, A., Haris, M., Zahid, Z., Jameel, M., Ahmad, A., Seth, C., Asseri, T., Hashem, M., Ahmad, F., 2024. *Polyalthia longifolia*-mediated green synthesis of zinc oxide nanoparticles: characterization, photocatalytic and antifungal activities. RSC Advances 14, 17535-17546.

Rodrigues, A., Gudiña, E., Abrunhosa, L., Malheiro, A., Fernandes, R., Teixeira, J., Rodrigues, L., 2021. Rhamnolipids inhibit aflatoxin production in *Aspergillus flavus* by causing structural damage in the fungal hyphae and down-regulating the expression of biosynthetic genes. International Journal of Food Microbiology 348, 109207.

Savi, G.D., Bortoluzzi, A.J., Scussel, V.M., 2013. Antifungal properties of zinc compounds against

toxigenic fungi and mycotoxin production. International Journal of Food Science and Technology 48, 1834-1840.

Shinde, S.S., 2015. Antimicrobial activity of ZnO nanoparticles against pathogenic bacteria and fungi. Science Medicine Central 3, 1033.

Subba, B., Bir, G., Bhandari, R., Parajuli, P., Thapa, N., Kandel, D.R., Mulmi, S., Shrestha, S., Malla, S.S., 2024. Antifungal activity of zinc oxide nanoparticles (ZnO NPs) on *Fusarium equiseti* phytopathogen isolated from tomato plant in Nepal. Heliyon e40198.

Tamim, H.H., Zaghloul, R.A., Elameen, T.M., Khalaphallah, R., 2024. Fungal synthesis of zinc oxide nanoparticles using *Aspergillus niger* for sustainable nanomaterial production and biological activity. SVU International Journal of Agricultural Sciences 6, 95-110.

Truong, H., Le, L., 2024. Exploring the physicochemical properties and antifungal activity of zinc oxide nanoparticles. Materials Technology 40(1), 2439832.

Vignesh, K., 2025. Green synthesis and characterization of zinc oxide nanoparticles using neem (*Azadirachta indica* L.) leaf extract. Asian Journal of Plant Pathology 19, 27-35.

Villagrán, Z., Anaya-Esparza, L.M., Velázquez-Carriles, C.A., Silva-Jara, J.M., Ruvalcaba-Gómez, J.M., Aurora Vigo, E.F., Rodríguez-Lafitte, E., Rodríguez-Barajas, N., Balderas-León, I., Martínez-Esquivias, F., 2024. Plant-based extracts as reducing, capping, and stabilizing agents for the green synthesis of inorganic nanoparticles. Resources 13, 70.

Wu, Q., Cen, F., Xie, Y., Ning, X., Wang, J., Lin, Z., Huang, J., 2025. Nanoparticle-based antifungal therapies: innovations, mechanisms and future prospects. PeerJ 13.

Zelekew, O.A., Aragaw, S.G., Sabir, F.K., Andoshe, D.M., Duma, A.D., Kuo, D.H., Chen, X., Desissa, T.D., Tesfamariam, B.B., Feyisa, G.B., Abdullah, H., 2021. Green synthesis of Co-doped ZnO via the accumulation of cobalt ion onto Eichhornia crassipes plant tissue and the photocatalytic degradation efficiency under visible light. Materials Research Express 8(2), 025010.